Isolating Intermediate $Mg_{11}Cu_6Al_{12}$ Phase in Ternary Mg-Cu-Al Alloy by Electrolytic Dealloying

Timothy Lee,[a] Jintao Fu,[a] Lin Wang,[a] Jiaxin Liu,[a] Samuel S. Welborn,[a,b] Johanna Nelson Weker,[b] and Eric Detsi[a,*]

[a] *Department of Materials Science & Engineering, University of Pennsylvania, Philadelphia PA 19104, USA*

[b] *Stanford Synchrotron Radiation Lightsource, SLAC National Accelerator Laboratory, Menlo Park, California 94025, United States*

** Email: detsi@seas.upenn.edu*

Abstract: While dealloying is widely used to create nanoporous materials, it has rarely been employed to isolate difficult-to-synthesize intermediate phases. Here we show how air-free, electrolytic dealloying at room temperature can be used to isolate the ternary intermetallic $Mg_{11}Cu_6Al_{12}$ phase. We create a ternary Mg-Cu-Al parent alloy containing the $Mg_{11}Cu_6Al_{12}$ compound and other phases, then subsequently remove these other phases via electrolytic dealloying to isolate the $Mg_{11}Cu_6Al_{12}$ phase. Isolated $Mg_{11}Cu_6Al_{12}$ phase exhibits ≈1 μm diameter rod-shaped microstructure. Phase and chemical analysis conducted using various techniques, including inductively coupled plasma and lab and synchrotron-based X-ray diffraction, show minimal impurities. This new approach to isolate the $Mg_{11}Cu_6Al_{12}$ phase can unlock its use in fundamental research and can be applied to other difficult-to-synthesize intermetallic compounds.

Key Words: intermetallic compounds, ternary compounds, electrochemistry, aluminum alloys, dealloying

Graphical Abstract:

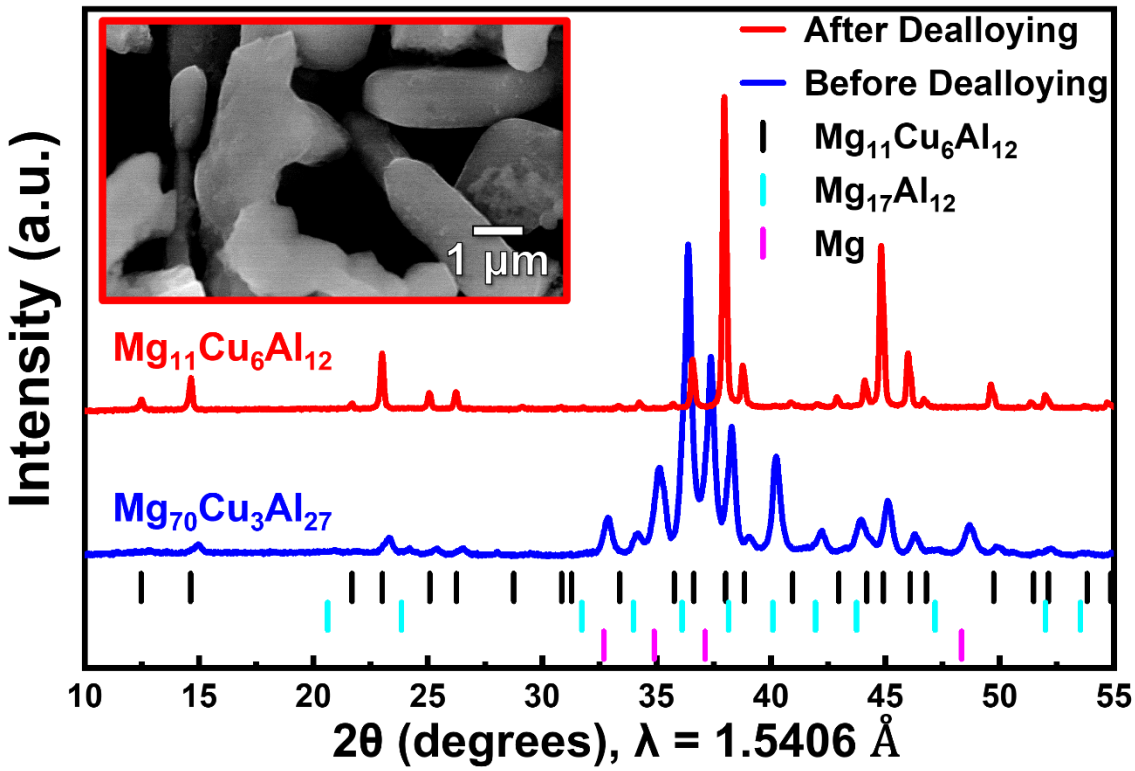

Dealloying, a selective alloy leaching process, has mostly been used as a nanostructuring method to create nanoporous materials with tunable size and high surface areas by selectively removing a sacrificial species from a parent alloy typically through free corrosion or electrolytic means.[1–5] Many of these nanoporous materials have various applications such as for catalysts[6,7], sensors[7,8], batteries [9–11], or hydrogen gas producers via hydrolysis.[12–15]. Advances have shown how dealloying of ternary parent alloys can create nanoporous binary intermetallics or alloys with electrocatalyst applications from stabilizing effects of the second element[16–19]. Furthermore, combining dealloying with additive manufacturing to create three-dimensional hierarchical nanoporous materials is another example of the broad versatility and resourcefulness of dealloying. [20–23]

However, we posit that dealloying is more versatile as a synthesis method than for just creating high-surface area structures. Here we show how the dealloying process can be extended beyond nanostructuring by using this method to entirely etch away the matrix of multicomponent alloys to isolate a desired intermediate phase present in this matrix. Intermediate phases formed in the matrix of multicomponent alloys usually exhibit remarkable mechanical, (electro)chemical, electronic, optical, and magnetic properties.[24–28] However, some intermediate phases only form at high temperatures and will decompose into other phases when the multicomponent alloy is brought to room temperature. Therefore, effective methods to isolate these intermediate phases are desirable. Specifically, we show that the ternary intermetallic phase, $Mg_{11}Cu_6Al_{12}$ (MCA), can be synthesized and isolated with minimal impurities via dealloying. This phase was chosen for investigation because of its challenging thermal synthesis method which has only been successfully demonstrated once in the literature by Berns et al.[29] Our strategy involves trapping the intermediate MCA phase in a parent alloy with more reactive phases, and subsequently removing these other reactive phases by room-temperature, air-free electrolytic dealloying. This new approach of dealloying to isolate the MCA phase can unlock it for fundamental research of its

properties and applications and can potentially apply to other types of difficult-to-synthesize intermetallic compounds.

To discuss the synthesis strategy for the MCA phase, some background clarification is needed. In the literature, MCA has only been successfully synthesized and extensively characterized once by Berns et al. in 2011 during their attempts to create the $Al_7Cu_3Mg_6$ phase from published ternary Al-Mg-Cu phase diagrams.[29–31] According to these ternary Al-Cu-Mg phase diagrams published from 2007, the $Al_7Cu_3Mg_6$ phase exists as a small, near-stochiometric point at 400°C, which decomposes into other Laves phases at room temperature.[29–31] Ternary phase diagrams generated using FactSage also show this decomposition occurring below 325°C as the phases present in the red region in **Figure 1** are different when comparing the Al-Cu-Mg ternary phase diagram at room temperature (**Figure 1a**) to 325°C (**Figure 1b**). Specifically, the phases noted in the red highlighted region of **Figure 1a** are hexagonal close-packed magnesium (HCP Mg), $Al_{12}Mg_{17}$, and other Al_xCu_yMg Laves phases (P63/mmc) (x=1.08-1.20, y=0.92-

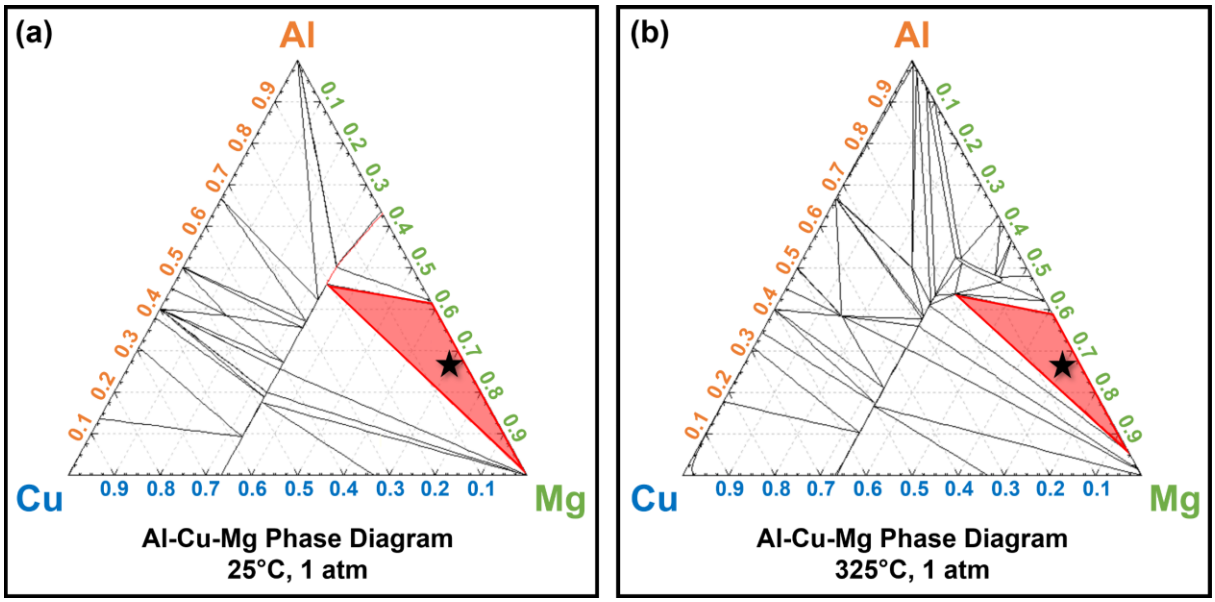

Figure 1. *Generated Al-Cu-Mg ternary phase diagrams at (a) 25°C and (b) 325°C from FactSage. Red highlighted region corresponds to (a) HCP-Mg, $Al_{12}Mg_{17}$, and other Laves phases, and (b) HCP-Mg, $Al_{12}Mg_{17}$, and $Al_7Cu_3Mg_6$ phases. Thus, thermal synthesis of $Al_7Cu_3Mg_6$ is difficult due to its decomposition at low temperature. The parent alloy composition $Mg_{70}Cu_3Al_{27}$ at. % in this work is marked with black star.*

0.80), while the phases noted in the red highlighted region of **Figure 1b** are HCP Mg, $Al_{12}Mg_{17}$, and $Al_7Cu_3Mg_6$ phases. This makes thermal synthesis of $Al_7Cu_3Mg_6$ phase difficult because of its decomposition at low temperatures and because of its existence as a near-stochiometric point where local variations in composition away from the target point will create other phases as impurities instead of pure $Al_7Cu_3Mg_6$ phase. Thus, we set out to synthesize the $Al_7Cu_3Mg_6$ phase like Berns et al. but by a different approach where we create a parent alloy in the red region in **Figure 1b** to contain the $Al_7Cu_3Mg_6$ phase with a composition away from the stochiometric point (i.e., moving towards the Mg-rich corner). Specifically, a parent alloy with composition $Mg_{70}Cu_3Al_{27}$ at. % is created (see supplemental information for experimental methods) as marked by the black star in **Figure 1a-b**; this composition is chosen for its distance from nearby phase boundaries to ensure a uniform parent alloy. We then remove the other phases present to attempt to arrive at the pure ternary intermetallic phase, which is either $Al_7Cu_3Mg_6$ phase by conventional phase diagrams or $Mg_{11}Cu_6Al_{12}$ as obtained by Berns et al. For this discussion, we will refer to our product as the $Mg_{11}Cu_6Al_{12}$ or MCA phase obtained by Berns et al. given the similarities in X-ray diffraction (XRD) patterns as will be shown and discussed later.

Electrolytic dealloying was performed using $Mg_{70}Cu_3Al_{27}$ at. % as the working electrode, Mg foil as the counter and reference electrodes, and all-phenyl complex (APC) as the electrolyte with an applied voltage of 1.0 V vs. Mg/Mg^{2+}. This voltage is chosen because it can remove both Mg and Al from the working electrode. A schematic for the dealloying cell is shown in **Figure 2a**. During this process, both the HCP Mg and $Mg_{17}Al_{12}$ phases are removed to leave behind MCA as a black powder at the working electrode. This powder is shown in **Figure 2b**. XRD analysis using Cu Kα radiation (λ = 1.5406 Å) before and after dealloying is shown in **Figure 2c**. Here the parent alloy with all three phases—Mg, $Mg_{17}Al_{12}$, and MCA—is shown before dealloying begins (**Figure 2c**, blue curve). After dealloying, only MCA is detected by lab-source powder XRD (red curve). A typical current profile for the dealloying process is shown in **Figure S1**; here the charge measured from the current during dealloying is associated with the amount of

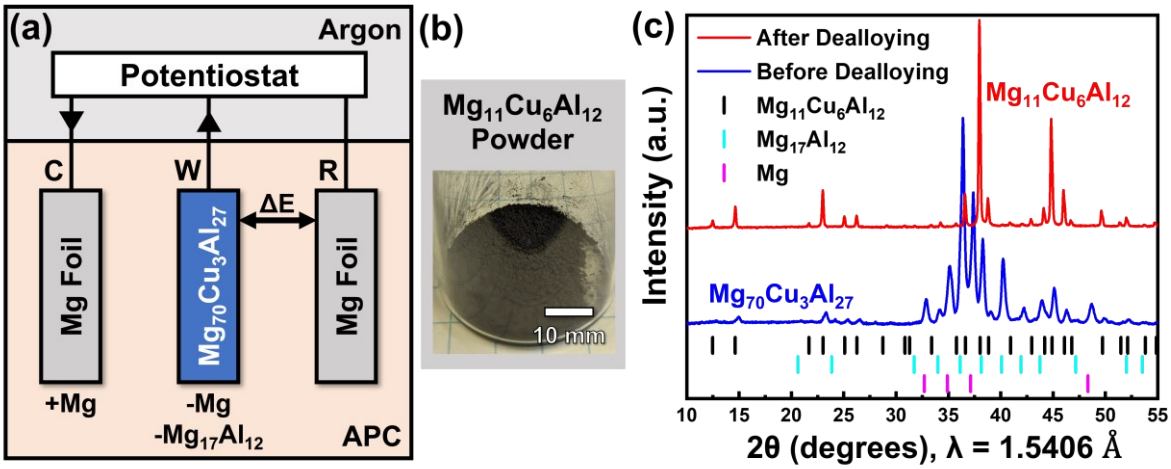

Figure 2. *(a) Schematic of cell used for electrolytic dealloying with Mg foils as the reference/counter (R/C) electrode and $Mg_{70}Cu_3Al_{27}$ at. % parent alloy as the working electrode (W). Mg and $Mg_{17}Al_{12}$ phases are removed from W via applied potential to produce (b) $Mg_{11}Cu_6Al_{12}$ (MCA) as black powder. (c) XRD characterization before and after dealloying process, showing phase-pure MCA can be obtained after dealloying. (λ = 1.5406 Å) (References: $Mg_{11}Cu_6Al_{12}$ ICSD ID 422849, Mg PDF #00-004-0770, $Al_{12}Mg_{17}$ PDF #01-073-1148)*

sacrificial materials dissolved and indicates ≈92 % completion rate when compared to the total expected charge capacity corresponding to removal of Al and Mg. This suggests a good yield or completion of the overall process (2058 mAh measured out of 2238 mAh expected). In the synthesis by Berns et al., high-temperature annealing at 500°C for ≈357 hours is required to collect phase-pure samples.[29] By using electrolytic dealloying, heating is only used to melt and create the parent alloy followed by a relatively short annealing and quenching process (3 hours) to lock the phases into the parent alloy. Here phase-pure samples as detected by lab-source XRD from **Figure 2c** can be collected after ≈257 hours and at room temperature, which unlocks scaling towards larger applications as well by lowering the energy requirement for synthesis.

We vary our dealloying approach to isolate MCA to provide more insight into this process and determine if a more pure phase product detected by XRD can be achieved. Here electrolytic dealloying is suitable because the desired phase can be made in a parent alloy with other more reactive components, and

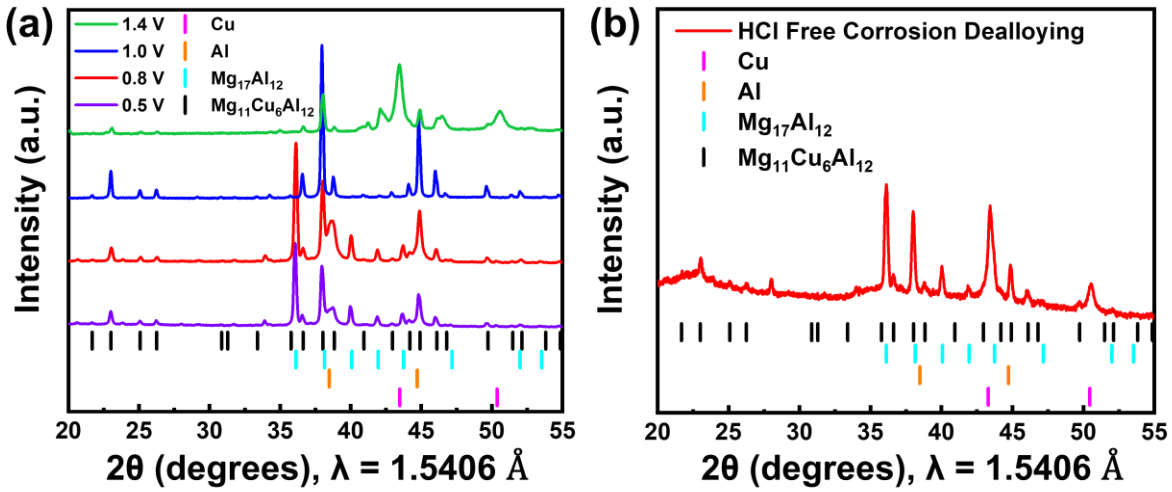

Figure 3. *Dealloyed product of $Mg_{70}Cu_3Al_{27}$ at. % (a) at different voltages or (b) using HCl for free-corrosion dealloying. Only dealloying at 1.0 V vs. Mg is shown to give the $Mg_{11}Cu_6Al_{12}$ phase. (λ = 1.5406 Å) (Reference: Al PDF #01-085-1327, Cu PDF #00-001-1241)*

a suitable electrolyte can be used to remove the more reactive components. Note that our electrolytic dealloying approach requires an applied voltage greater than 0.71 V vs. Mg/Mg^{2+}—the difference between the equilibrium potentials of Al/Al^{3+} (-1.662 V vs. SHE) and Mg/Mg^{2+} (-2.372 V vs. SHE) metal[32]—to account for the overpotential required for shuttling Al. Furthermore, the Cu atoms present in $Mg_{11}Cu_6Al_{12}$ make the ternary phase more noble and unable to be electrolytically removed at this potential. As shown in **Figure 3a**, lower voltages such as 0.5 or 0.8 V vs. Mg/Mg^{2+} (black and red curve) will result in partial dealloying in which both $Mg_{17}Al_{12}$ and pure face-centered cubic (FCC) Al phases are detected. The latter Al phase comes from the removal of Mg from $Mg_{17}Al_{12}$ resulting in nanoporous Al as expected from previous work.[12,15] However, there is a maximum higher voltage which is reached at 1.4 V vs. Mg/Mg^{2+} (green curve), since the destruction of the MCA phase is observed by the detection of the pure Cu phase. Similar destruction of the MCA phase using free corrosion dealloying with 1 M HCl also results in detection of pure Cu and $Mg_{17}Al_{12}$ phases by XRD as shown in **Figure 3b**. This further supports the significance of

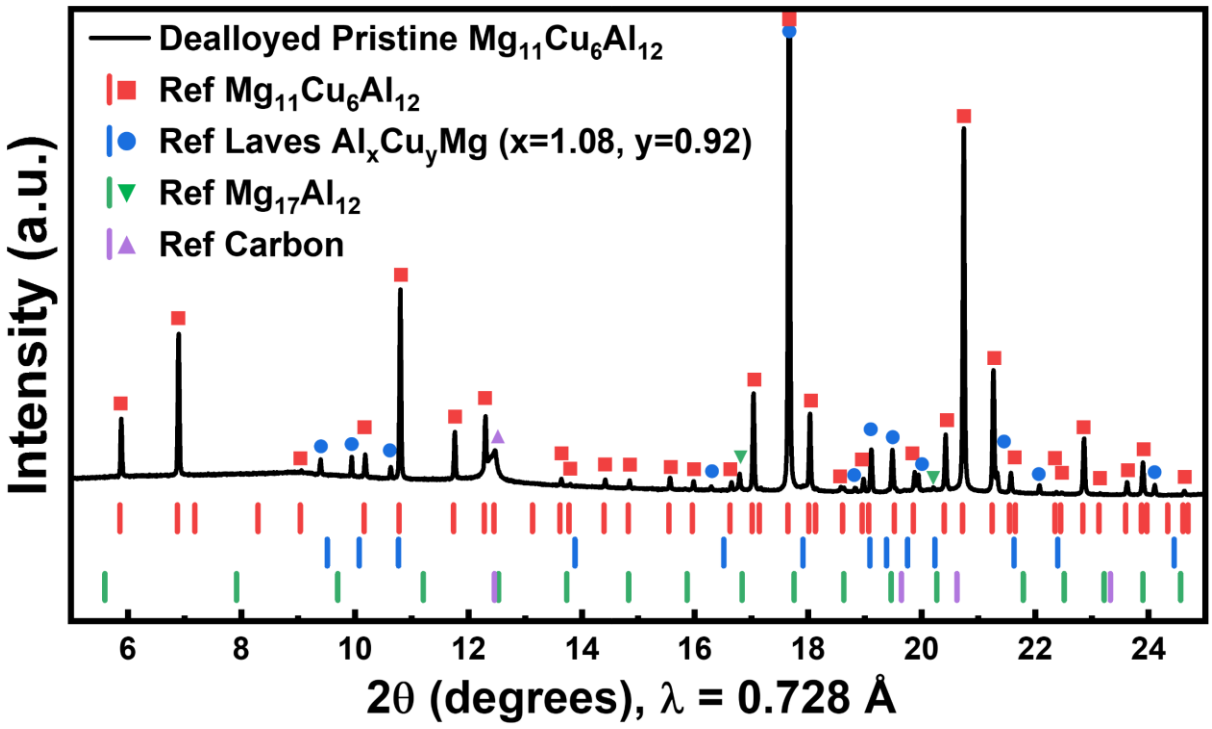

Figure 4. *Synchrotron XRD analysis of dealloyed MCA powder (black curve) with reference stick patterns for $Mg_{11}Cu_6Al_{12}$ (red, square), Laves P63/mmc Al_xCu_yMg (x=1.08, y=0.92) (blue, circle), $Mg_{17}Al_{12}$ (green, upside-down triangle), and carbon (purple, triangle). All peaks detected are assigned with corresponding shape and color. The carbon peak is from a small amount of carbon additive. (λ = 0.728 Å) (Reference: Al_xCu_yMg (x=1.08, y=0.92) ICSD ID 199479, Carbon ICSD ID 51381). Under this higher resolution XRD, the Laves phase is detected as impurity, which originates from MCA decomposition at room temperature.*

using the electrolytic dealloying strategy at 1.0 V vs. Mg/Mg^{2+} as this was the most suitable method for isolating the MCA phase.

Synchrotron XRD (SXRD) is used to examine the phase composition of MCA with higher resolution to distinguish any impurity phases that may not have appeared from the lab-source XRD. Phase analysis by SXRD on the dealloyed MCA powder is shown in **Figure 4**. All peaks that can be detected were assigned to its corresponding phase. For the $Mg_{11}Cu_6Al_{12}$ phase, many peaks exist and can be visibly assigned, while some peaks with extremely low intensities (such as at ≈7.2° and ≈8.3°) are not detected. A very small amount of starting material $Mg_{17}Al_{12}$ phase remains as noted by the small peaks at ≈16.8° and ≈20.3°. The main impurity phase detected is most likely the Laves (P63/mmc) Al_xCu_yMg phase, which

comes from decomposition of MCA at room temperature as mentioned earlier from **Figure 1a**. Note that this Laves phase can represent a broad composition range where the amount of Al (x = 1.08-1.20) and Cu (y= 0.92-0.80) can vary; this variation in Al and Cu can cause changes in lattice parameters that results in peak shifting when comparing to the reference pattern used where x=1.08 and y=0.92.[33] Such peak shifting is more intense for higher degree peaks and is a known phenomenon that has been noted before in the literature for Cu/Al solid solutions.[34] Thus, the peak assignment represented by blue dots varies from the reference represented by blue sticks as shown in **Figure 4** for the Laves phase. Note that this Laves phase is not seen on lab-source XRD in **Figure 2c**, and future optimizations to the parent alloy creation and quenching process can further minimize its presence.

Microstructural characterization of the MCA product is shown in **Figure 5a-b**. Scanning electron microscopy (SEM) shows that the final MCA product is not nanoporous at higher magnification as shown in **Figure 5b**; instead, it is rod shaped with diameter ≈1 micron. This rod-like structure differs from most dealloyed products commonly exhibiting a nanoporous structure, but such a structure has been noted before in the literature.[35] Energy-dispersive X-ray spectroscopy (EDX) mapping is shown in **Figure 5c-f** for elemental composition characterization. Here the overall elemental composition map is relatively uniform for all three elements, while the overlay shows Al as the element with the highest concentration. EDX and inductively coupled plasma optical emission spectroscopy (ICP-OES) are also conducted before and after dealloying in **Figure 5g** to show the change in composition. It is important to note that when Berns et al. first reported on the MCA phase, they note that $Mg_9Cu_6Al_{14}$ is also a possible composition whereby replacing two Mg atoms with Al gives the same crystal structure.[29] They conclude a mixture of both compositions is possible based on several factors such as a bond length analysis. Based on EDX and ICP-OES, the MCA product is within the appropriate at. % range of the two ideal compositions.

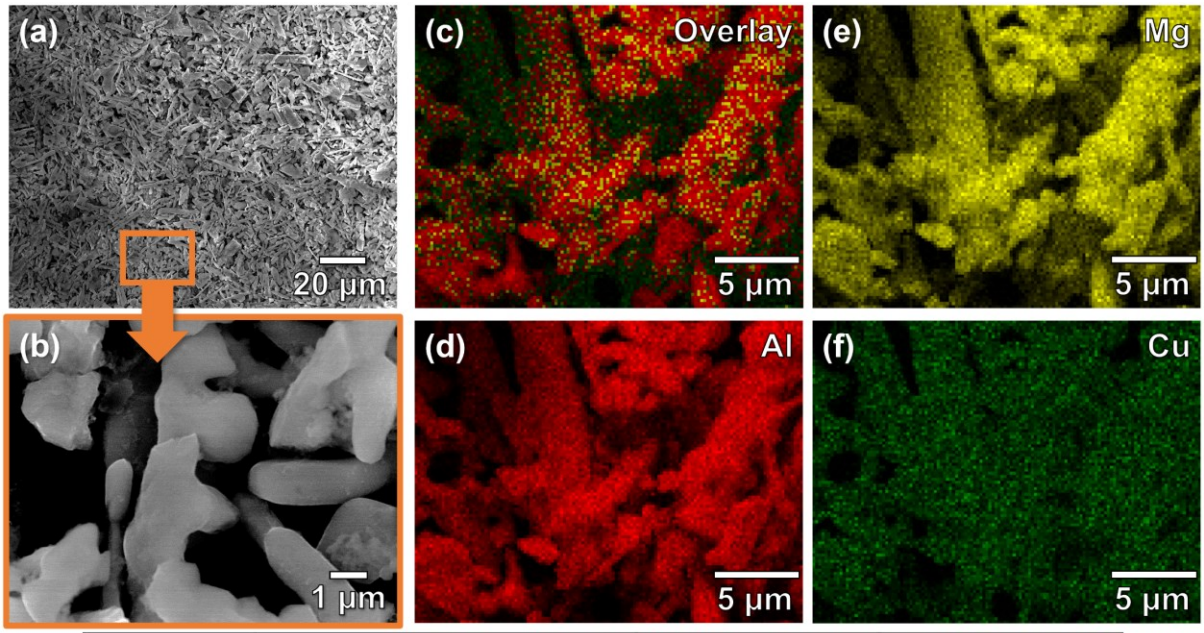

(g)

	Ideal Compositions		Before Dealloying		After Dealloying	
Elements	$Mg_9Cu_6Al_{14}$	$Mg_{11}Cu_6Al_{12}$	EDX	ICP	EDX	ICP
Mg (at. %)	31 %	38 %	69 %	71 %	34 %	38 %
Al (at. %)	48 %	41 %	28 %	26 %	46 %	45 %
Cu (at. %)	21 %	21 %	3 %	3 %	20 %	17 %

Figure 5. *(a-b) SEM imaging showing microstructure of MCA which consists of rod-shaped structure with diameter around 1 micron. (c-f) EDX mapping showing bulk distribution of elements. All three elements (Mg, Cu and Al) are uniformly distributed with Al as the element with the highest concentration. (g) Compositional analysis showing ideal elemental compositions of MCA phase and compositions before and after dealloying characterized through EDX and ICP-OES. The composition of MCA product obtained after dealloying falls within the range of two ideal phases.*

In conclusion, while dealloying is a versatile synthesis method when it comes to creating nanostructures, here we show how electrolytic dealloying can be used to overcome the difficulty in thermal synthesis and create intermediate phases using the ternary intermetallic MCA phase as an example. Synchrotron phase characterization of MCA from electrolytic dealloying reveals only a small amount of an impurity phase, which is likely the Laves (P63/mmc) Al_xCu_yMg phase. This phase is expected to come from room-temperature decomposition of MCA. Meanwhile, microstructural characterization shows ≈1 micron diameter rod shapes instead of the typical nanoporous structure. Furthermore, this phase can be

made using significantly less energy in room-temperature electrolytic dealloying compared to the traditional thermal synthesis process requiring 500°C annealing for 357 hours, which unlocks this phase for fundamental research and potential applications.

Acknowledgments

The authors are thankful to the National Science Foundation (NSF) for their financial support via NSF-CAREER (Award Number: CMMI-2047851, Eric Detsi) and NSF GRFP (Award Number: DGE-1845298, Timothy Lee). This work was carried out in part at the Singh Center for Nanotechnology, part of the National Nanotechnology Coordinated Infrastructure Program, which is supported by the NSF grant NNCI-1542153. Use of the Stanford Synchrotron Radiation Lightsource, SLAC National Accelerator Laboratory, is supported by the U.S. Department of Energy, Office of Science, Office of Basic Energy Sciences under Contract No. DE-AC02-76SF00515.

Declaration of Competing Interest

There is no competing interest to declare.

References

[1] H.J. Qiu, L. Peng, X. Li, H.T. Xu, Y. Wang, Corros. Sci. (2015).

[2] I. McCue, E. Benn, B. Gaskey, J. Erlebacher, Annu. Rev. Mater. Res. (2016).

[3] T. Song, M. Yan, M. Qian, Corros. Sci. (2018).

[4] J. Weissmüller, K. Sieradzki, MRS Bull. (2018).

[5] M. Hakamada, M. Mabuchi, Scr. Mater. (2007).

[6] Y. Ding, M. Chen, MRS Bull. (2009).

[7] A. Wittstock, J. Biener, M. Bäumer, Phys. Chem. Chem. Phys. (2010).

[8] H.J. Qiu, X. Li, H.T. Xu, H.J. Zhang, Y. Wang, J. Mater. Chem. C (2014).

[9] J. Niu, M. Song, Y. Zhang, Z. Zhang, J. Magnes. Alloy. (2021).

[10] Q. Sang, S. Hao, J. Han, Y. Ding, EnergyChem (2022).

[11] X. Wu, G. He, Y. Ding, Electrochem. Energy Rev. (2020).

[12] J.S. Corsi, J. Fu, Z. Wang, T. Lee, A.K. Ng, E. Detsi, ACS Sustain. Chem. Eng. 7 (2019) 11194–11204.

[13] J. Fu, J.S. Corsi, S.S. Welborn, V. Basile, L. Wang, A.K. Ng, E. Detsi, ACS Sustain. Chem. Eng. (2021).

[14] J. Fu, Z. Deng, T. Lee, J.S. Corsi, Z. Wang, D. Zhang, E. Detsi, ACS Appl. Energy Mater. 1 (2018) 3198–3205.

[15] T. Lee, J.S. Corsi, L. Wang, E. Detsi, ACS Appl. Energy Mater. (2021).

[16] P. Mani, R. Srivastava, P. Strasser, J. Power Sources 196 (2011) 666–673.

[17] C. Zhang, Z. Xie, X. He, P. Liang, Q. Zeng, Z. Zhang, CrystEngComm 20 (2018) 6900–6908.

[18] J. Snyder, P. Asanithi, A.B. Dalton, J. Erlebacher, Adv. Mater. 20 (2008) 4883–4886.

[19] L. Lührs, J. Weissmüller, Scr. Mater. (2018).

[20] A. Chuang, J. Erlebacher, Materials (Basel). (2020).

[21] T. Fujita, Sci. Technol. Adv. Mater. (2017).

[22] S. Mooraj, S.S. Welborn, S. Jiang, S. Peng, J. Fu, S. Baker, E.B. Duoss, C. Zhu, E. Detsi, W. Chen, Scr. Mater. (2020).

[23] C. Zhu, Z. Qi, V.A. Beck, M. Luneau, J. Lattimer, W. Chen, M.A. Worsley, J. Ye, E.B. Duoss, C.M. Spadaccini, C.M. Friend, J. Biener, Sci. Adv. (2018).

[24] J. Zhang, Y.N. Huang, C. Mao, P. Peng, Solid State Commun. 152 (2012) 2100–2104.

[25] F. Hadef, J. Magn. Magn. Mater. 419 (2016) 105–118.

[26] M.G. Blaber, M.D. Arnold, M.J. Ford, J. Phys. Condens. Matter (2010).

[27] D. Makwana, P.P. Bhingole, Mater. Today Proc. 27 (2020) 1319–1323.

[28] S. Lv, F. Meng, Q. Yang, K. Guan, J. Meng, Mater. Des. 208 (2021) 109904.

[29] V.M. Berns, T.E. Stacey, M. Sapiro, D.C. Fredrickson, Eur. J. Inorg. Chem. (2011) 3936–3949.

[30] T. Buhler, S.G. Fries, P.J. Spencer, H.L. Lukas, J. Phase Equilibria 1998 194 19 (1998) 317–333.

[31] V. Raghavan, J. Phase Equilibria Diffus. 2007 282 28 (2007) 174–179.

[32] P. Vanysek, Hand B. (2000).

[33] E.V. Mel'nik, V.V. Kinzhibalo, Russ. Metall. (1981) 154–158.

[34] S. Juan, G. Feng, G. Xiaobo, F. Haiquan, J. Alloys Compd. 854 (2021) 156209.

[35] S. Liu, X. Bian, J. Liu, J. Wang, M. Yu, Y. Yang, R. Fan, Intermetallics (2018).